

Effects of laser pulse energy on surface microstructure and mechanical properties of high carbon steel

XIONG Yi(熊毅)^{1,2}, HE Tian-tian(贺甜甜)³, LI Peng-yan(李鹏燕)¹,
CHEN Lu-fei(陈路飞)¹, REN Feng-zhang(任凤章)^{1,2}, Alex A. Volinsky⁴

1. School of Materials Science and Engineering, Henan University of Science and Technology, Luoyang 471023, China;
2. Collaborative Innovation Center of Nonferrous Metals, Luoyang 471023, China;
3. Institute of Metal Research, Chinese Academy of Sciences, Shenyang 110016, China;
4. Department of Mechanical Engineering, University of South Florida, Tampa FL 33620, USA

© Central South University Press and Springer-Verlag Berlin Heidelberg 2015

Abstract: Surface microstructure and mechanical properties of pearlitic Fe–0.8%C (mass fraction) steel after laser shock processing (LSP) with different laser pulse energies were investigated by scanning electron microscopy (SEM), transmission electron microscopy (TEM), X-ray diffraction (XRD) and microhardness measurements. After LSP, the cementite lamellae were bent, kinked and broken into particles. Fragmentation and dissolution of the cementite lamellae were enhanced by increasing the laser pulse energy. Due to the dissolution of carbon atoms in the ferritic matrix, the lattice parameter of α -Fe increased. The grain size of the surface ferrite was refined, and the microstructure changed from lamellae to ultrafine micro-duplex structure (ferrite (α)+cementite (θ)) with higher laser pulse energy, accompanied by the residual stress and microhardness increase.

Key words: pearlitic steel; laser shock processing; microstructure; microhardness; residual stress

1 Introduction

It is well known that mechanical properties of metals are closely related to their microstructure. Some of the failure mechanisms, such as wear and friction, fatigue and corrosion, are sensitive to the surface state of materials, as failure always starts with the surface damage, thus the surface structure and state directly affect the materials life and performance. In order to prolong the service life and meet the requirements in harsh environments, it is important to improve the surface physical properties of materials. Laser shock processing (LSP) is a new surface treatment technique for improving metal mechanical properties [1–2]. The generated shock wave can produce severe plastic deformation, as well as deep compressive residual stresses of several hundreds of MPa by exposing metallic samples to high power density and short pulse laser beam. LSP can improve fatigue life [3], corrosion [4], wear resistance [5] and other mechanical properties [6] of metals and alloys. It has applications in the aerospace, automotive, marine, and other industries.

Carbon steel is one of the most widely used structural materials. LSP has been shown to harden the surface and improve mechanical properties of low carbon [7–8] and stainless steels [9–10]. However, only a few studies have focused on the LSP effects on high carbon steels properties [11]. High carbon steels are widely used in the industry. Therefore, a basic understanding of the underlying mechanism for microstructure evolution and the corresponding mechanical properties by ultra-high-strain-rate plastic deformation becomes more and more crucial. The results discussed in this work will provide the technical support for broadening industrial applications of high carbon steels.

2 Materials and experimental procedure

The material used in this work was commercial high carbon steel (Fe–0.8%C). To ensure the full evolution of pearlite, all specimens were vacuum annealed at 1273 K for 30 min and then placed into a salt bath furnace at 873 K for 30 min. This was followed by water cooling outside the furnace. Before LSP, the samples were cut into discs with $d20\text{ mm}\times 2\text{ mm}$ dimensions.

Foundation item: Projects(50801021, 51201061) supported by the National Natural Science Foundation of China; Project(144200510009) supported by the Henan Province Program for Science and Technology Innovation Excellent Talents, China; Project(152102210077) supported by the Science and Technology Project of Henan Province, China; Project(2015XTD006) supported by the Science and Technology Innovation Team of Henan University of Science and Technology, China

Received date: 2014–10–29; **Accepted date:** 2015–04–20

Corresponding author: XIONG Yi, PhD; Tel: +86–379–64231269; E-mail: xy_hbby@163.com

The laser used for shock processing was a solid state Nd:glass phosphate laser, operating at a wave length of 1.064 μm , and a pulse duration of about 10 ns, measured at the full width half maximum. The laser beam spot size on the sample was 3 mm. Samples were submerged into a water bath where they were treated with LSP. A water layer with a thickness of about 1 mm was used as the transparent confining layer and the 3M professional aluminum tape with a thickness of 100 μm was used as an absorbing layer to protect the sample surface from the thermal effects. The samples were treated by the 4 LSP impacts with different laser pulse energies of 2 J and 6 J, respectively. The processing parameters used in the LSP are listed in Table 1. During multiple LSP impacts, the laser beam was perpendicular to the sample surface, kept at the same location on the sample, and the Al tape was replaced after each of multiple LSP impacts.

Table 1 Processing parameters used in LSP

Parameter	Value
Output beam divergence/mrad	≤ 2
Spot diameter/mm	3
Pulse energy/J	2 or 6
Pulse width/ns	< 15
Repetition rate/Hz	5
Laser wavelength/nm	1064
Beam profile	Top hat
Pulse to pulse energy stability/%	< 1

Field-emission scanning electron microscopy (FESEM, QUANTA FEG650) was used for surface morphology analysis. The specimens were etched using 4% nital solution after LSP. The microstructure of the processed specimens was examined using transmission electron microscopy (TEM, JEM-2010) operated at 200 kV. Thin foil, mechanically polished down to 40 μm , was utilized for TEM samples prepared by a double jet electrolytic thinning technique (30 V, 50 mA) in a mixture of 93% (volume fraction) acetic acid and 7% (volume fraction) perchloric acid. Liquid nitrogen was used for cooling during the thinning process, with the temperature rising no higher than 243 K.

D8 ADVANCE X-ray diffractometer with Cu K_{α} radiation was used to determine the phase changes. The final lattice parameter of the ferrite was obtained by means of extrapolation using the least squares method.

The residual stresses in the samples with and without LSP were measured using XRD with the $\sin^2\theta$ method. The X-ray beam diameter was about 2 mm. The X-ray source was Cr K_{α} , and the diffraction plane was the α phase (211) plane. The feed angle of the ladder

scanning was $0.1(^{\circ})/\text{s}$. The scanning starting and terminating angles were 152° and 160° , respectively. For the depth profile stress measurements, the specimen surface was removed incrementally by electropolishing. Microhardness of the laser processed regions was measured by the MH-3 Vickers microhardness tester (2 N load, 10 s holding time). An average microhardness value was determined based on five indentation measurements.

3 Results and discussion

3.1 Microstructure evolution

The initial fully pearlitic microstructure of the as-received Fe–0.8%C (mass fraction) steel is shown in Fig. 1(a). The alignment of the cementite lamellae is orderly and the lamellae are parallel to each other. The thickness of cementite lamellae is about 30 nm and the average lamellae spacing is about 150 nm, as seen in Fig. 1(b). Figures 1(c) and (d) show typical SEM images of the Fe–0.8%C (mass fraction) steel after LSP with the laser pulse energy of 2 J and 6 J, respectively, and the impact direction is from top to bottom. The plastic deformation of the sample after LSP is mainly due to the deformation of the cementite lamellae. After LSP with a low energy of 2 J, as seen in the area *A* of Fig. 1(c), a large number of cementite lamellae were kinked in order to coordinate severe plastic deformation of the ferrite. Part of the cementite lamellae are fractured, and the shape of the cementite is a short bar, or an ellipse, as seen in the area *B* of Fig. 1(c). The occurrence of fragmentation in a small portion of cementite can be also found in the area *C* of Fig. 1(c). The cementite lamellae shear in a regular way in the area *D* of Fig. 1(c). After LSP with a high energy, as seen in Fig. 1(d), due to the different arrangement of cementite lamellae, the lamellae are bent in the impact direction to coordinate the deformation, which can be found in the area *A* of Fig. 1(d). However, the lamellae were kinked or fractured perpendicular to the impact direction. With the increasing laser pulse energy, fragmentation of the cementite lamellae is increased and most cementite lamellae are transformed to the cementite particles, about 250 nm in diameter, as seen in the area *B* of Fig. 1(d).

Figures 2(a) and (b) show TEM images of the Fe–0.8%C steel at the top surface after LSP with the laser pulse energies of 2 J and 6 J, respectively. It can be seen that the original cementite lamellae disappeared and were almost completely fragmented. After LSP with the laser pulse energy of 2 J, fragmentation of the cementite lamellae is not complete and the shape of most cementite is a short bar. The size of the fragmented cementite particles is about 100 nm. Meanwhile, the ferrite is elongated with the grain size of about 500 nm. With the

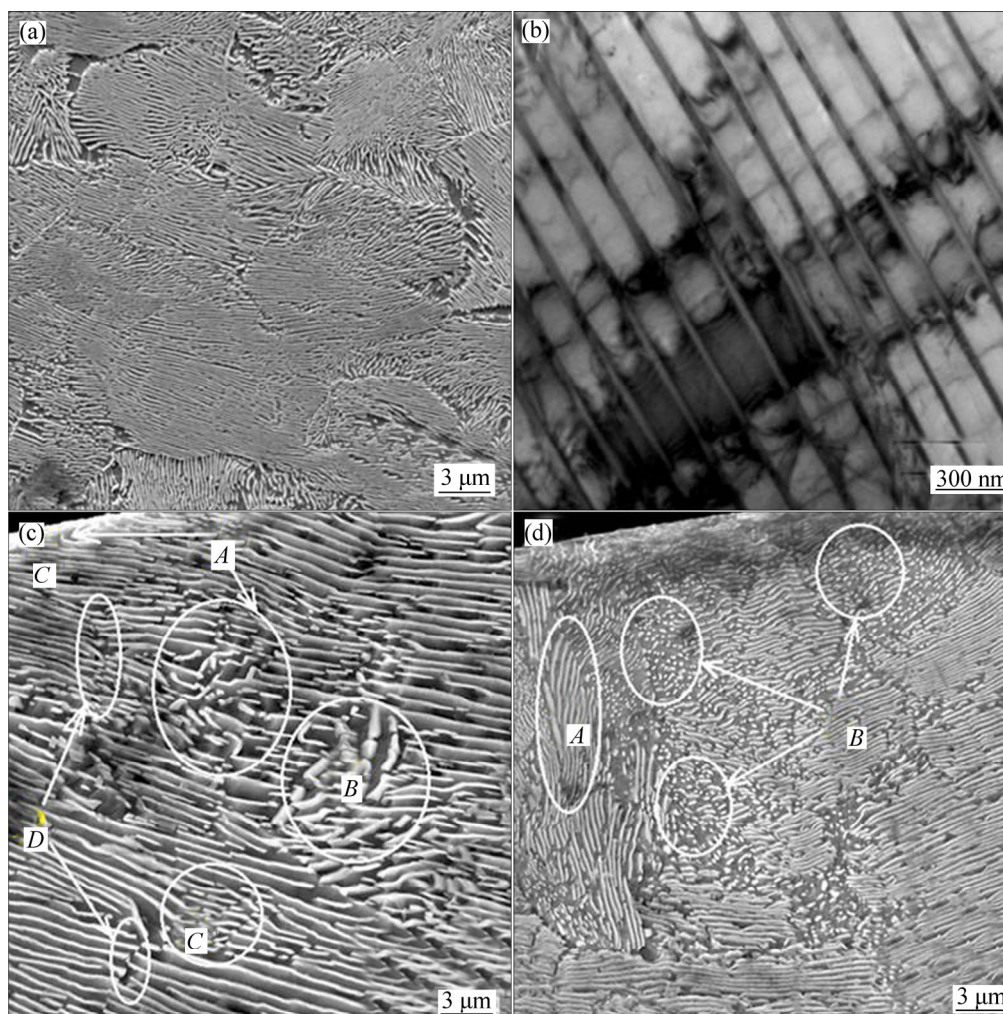


Fig. 1 SEM (a), TEM (b) of pearlite microstructure before LSP and SEM micrographs of Fe–0.8%C (mass fraction) steel after different LSP pulse energies of 2 J (c) and 6 J (d)

increasing laser pulse energy, fragmentation of the cementite lamellae is increased. However, the amount of the cementite obviously decreases and the average diameter of the cementite particles is now 300 nm. Meanwhile, the ferrite grains are equiaxed, with an average grain size of 250 nm. Figures 2(c) and (d) show TEM images of the samples up to a depth of approximately 150 μm from the top surface after LSP with the laser pulse energies of 2 J and 6 J, respectively. Note that after LSP with the laser pulse energy of 2 J, the cementite lamellae are fractured, with most of lamellae still present. In some local areas, the shape of the cementite is a short bar or an ellipse, indicating the occurrence of the cementite lamellae fragmentation. Meanwhile, more dislocations are formed, and dislocation lines pile-up contributes to the formation of dislocation tangles and dense dislocation cells, finally leading to the formation of subgrains with the grain size of about 300 nm, as seen in Fig. 2(c). Most of the

original cementite lamellae disappeared with the increasing laser pulse energy. Dislocation tangles are increased and a large number of dislocation cells can be found in Fig. 2(d). At the same time, the size of elongated ferrite grain is about 400 nm. Figures 2(e) and (f) show TEM images of the samples up to a depth of approximately 300 μm from the top surface after LSP with the laser pulse energies of 2 J and 6 J, respectively. After LSP with a low energy of 2 J, the cementite is still lamella in shape; however, a large number of dislocation lines are formed on the ferrite matrix, as seen in Fig. 2(e). After LSP with a high energy, dislocation density increases significantly with dislocation tangles, leading to the cementite lamellae breakage. Also, the subgrain boundary between the cementite lamellae can be observed in Fig. 2(f).

Figure 3 shows XRD patterns of the pearlitic Fe–0.8%C steel after LSP with different energies. Compared with the as-received sample, the α -Fe peaks

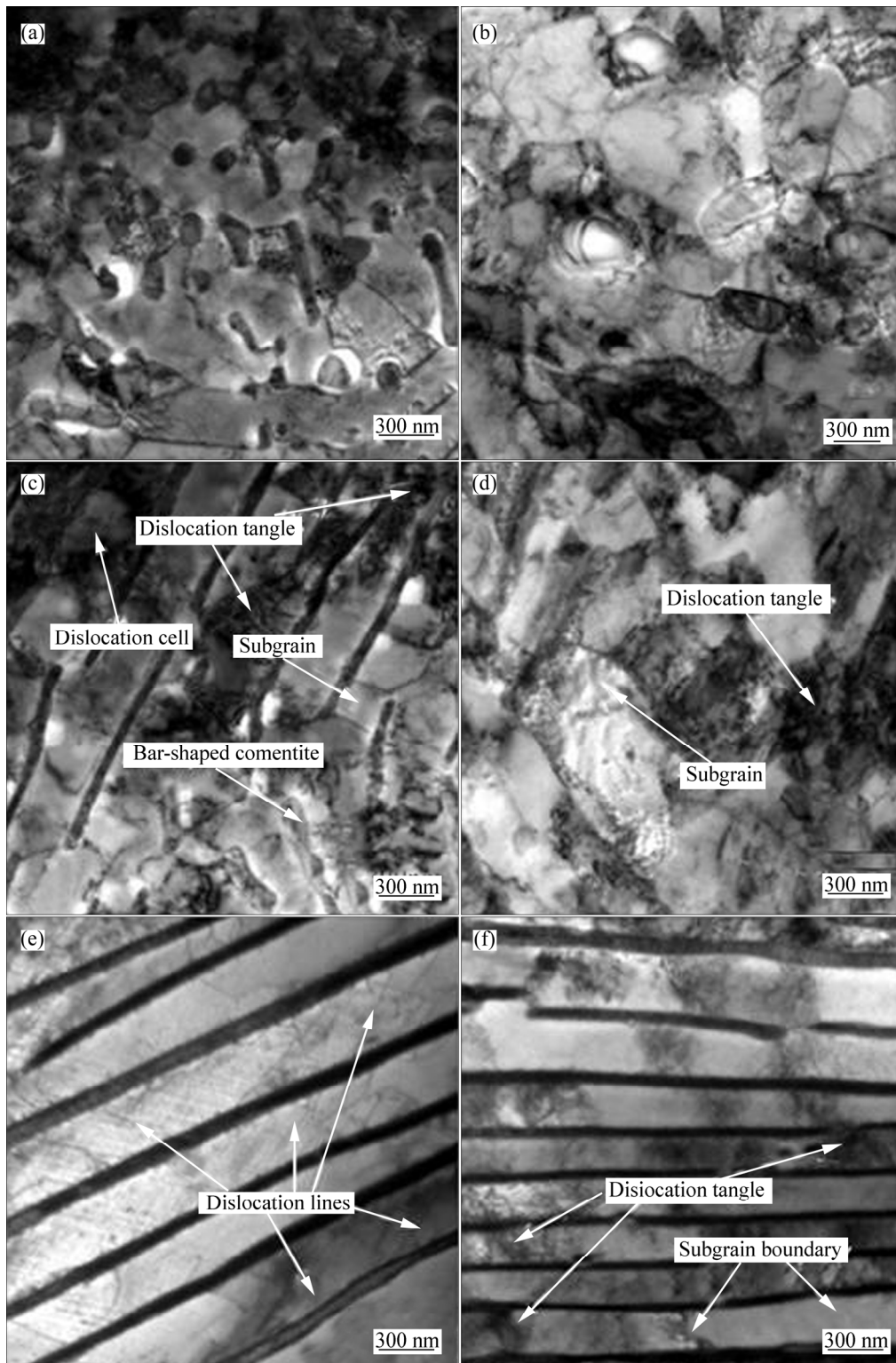


Fig. 2 Typical TEM images of Fe–0.8%C steel after LSP with laser pulse energies of 2 J and 6 J: (a)–(b) At the top surface; (c)–(d) At 150 μm depth from top surface; (e)–(f) At 300 μm depth from top surface

shift to smaller diffraction angles after LSP. The higher the LSP pulse energy is, the more significant the left shift of the α peaks is. The lattice parameter of α -Fe is 0.28570 nm in the Fe–0.8%C steel. After LSP with the energies of 2 J and 6 J, the lattice parameters of α -Fe are 0.28582 nm and 0.28625 nm, respectively. The lattice

parameters of α -Fe increase with the LSP pulse energy. The carbon content in the pearlite ferrite after different LSP pulse energies can be estimated according to the relationship between the lattice parameter and the carbon constant of α -Fe given by FU et al [12]. Corresponding changes of the carbon mass fraction in α -Fe are 0.03%

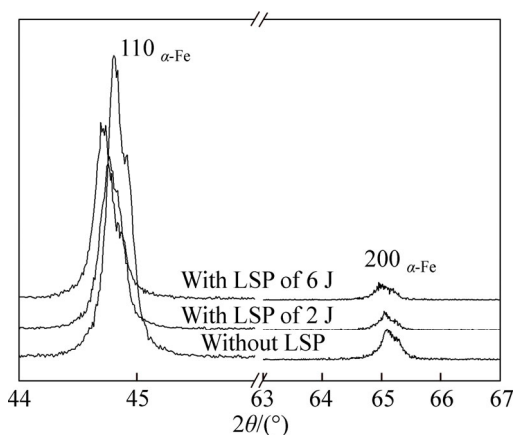


Fig. 3 Changes of XRD peak position of α -Fe in pearlitic Fe-0.8%C steel before and after LSP with different pulse energies

and 0.14% after 2 J and 6 J LSP, respectively. This indicates that the cementite dissolution results in the increase of the carbon constant, leading to the α -Fe lattice parameter increasing. The higher the LSP pulse energy is, the more the cementite dissolved is. Similar changes of the α -Fe lattice parameter were reported in other studies for cold-rolled pearlitic steels [13]. LSP is a cold processing technique [14], and it is different from laser cladding and laser welding [15–16]. Under the effect of the laser shock wave, the cementite lamella are bent, kinked, fragmented and even partially dissolved to coordinate severe plastic deformation of the ferrite.

3.2 Microhardness

Figure 4 shows microhardness values of the pearlitic Fe-0.8%C steel near the surface after different LSP pulse energies. It can be seen that microhardness increases with the LSP pulse energy and microhardness in the impact center is obviously improved compared with the corresponding values at the edge. This is because the stress induced by the shock wave has a

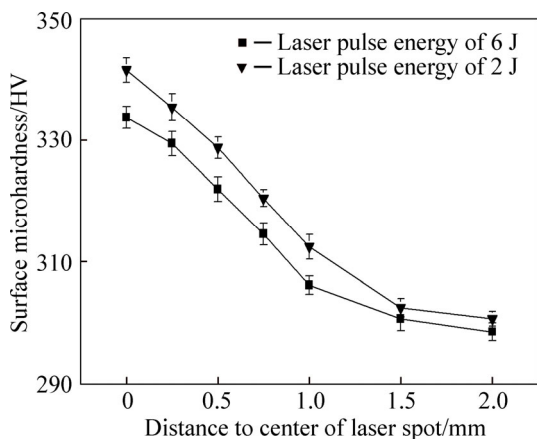


Fig. 4 Microhardness of pearlitic Fe-0.8%C steel after different LSP pulse energies

Gaussian distribution due to the intrinsic character of the laser pulse energy. In the impact center, severe plastic deformation occurred, so the microhardness is higher than that in other regions. After LSP with the laser pulse energy of 2 J, the microhardness increased by 11% from HV 300 (before LSP) to HV 334 in the impact center. With the laser pulse energy increasing to 6 J, the microhardness is HV 342, which is a 14% increase compared with the samples without LSP. In our previous work, the microhardness of the ultrafine-grained high carbon steel after LSP increased by about 30% [11]. However, in the present work, the increase of microhardness is lower than 15%. LSP causes severe plastic deformation, thus the microstructure of the Fe-0.8%C steel results from the slip and pile-up of high density dislocations, leading to dislocations pinning. Therefore, after LSP, the surface microhardness increases mainly due to dislocation strengthening. Meanwhile, the fragmentation of the cementite lamellae decreases the microhardness. According to the SEM/TEM results, the ferrite is obviously refined after LSP and the grain size of the ferrite decreases with the laser pulse energy increasing. Due to the joint action of work hardening, fragmentation of the cementite lamellae and grain refinement, the microhardness in the impact center increases slowly. Also, the microhardness is higher after the higher energy LSP.

3.3 Residual stress

The measured residual stresses with and without four LSP impacts with different laser pulse energy in depth direction are shown in Fig. 5. It can be seen that the untreated regions are approximately in the zero stress state, indicating that the effect of initial stress on the shock waves can be ignored [17]. From Fig. 5, it should be noted that the pulse energy has a significant effect on the magnitude of the residual stress due to LSP. The maximum compressive residual stress is located at the treated surface and the value increases with the pulse energy. After LSP with the laser pulse energies of 2 J and 6 J, the maximum residual stresses are -212 MPa and -267 MPa, respectively. It is well known that the compressive residual stresses near the specimen surface are generated due to the local plastic deformation after LSP. Severe deformation results from the higher pulse energy. Hence, the residual stress increases with the laser pulse energy. Meanwhile, the value of the compressive residual stress decreases gradually with the distance to the treated surface. Plastically affected depth is 680 μ m and 850 μ m after LSP with the laser pulse energies of 2 J and 6 J, respectively. After LSP, the compressive residual stress exists in the near surface layer, however, after shot peening, the maximum compressive residual stress is at the subsurface. This difference is mainly due to the

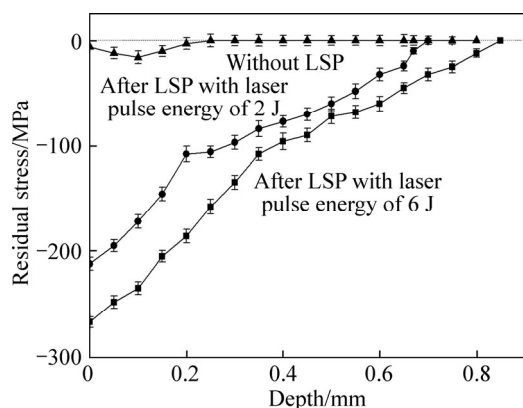


Fig. 5 Residual stress profiles of samples before and after different LSP pulse energies in depth direction

thermal effects [18–19].

The shock pressure exerted on the sample surface during LSP results in the compressive residual stresses. The presence of compressive residual stresses will have a beneficial effect on the fatigue performance [20]. It is well known that fatigue cracks mostly originate at the surface of materials, while a compressed surface layer will inhibit the crack initiation and growth. Hence, the compressive stresses at the surface may improve the fatigue performance of the specimen after LSP.

4 Conclusions

1) After LSP, the cementite lamellae are bent, kinked and broken into particles. With increasing LSP pulse energy, the degree of deformation and dissolution of the cementite lamellae are enhanced. After LSP with the laser pulse energy of 6 J, the ultrafine micro-duplex structure, with 300 nm equiaxed ferrite grains and 250 nm cementite particles, is formed on the surface of the samples.

2) After different LSP pulse energy treatments, the lattice parameter of α -Fe increases from 0.28570 nm to 0.28582 nm (2 J), to 0.28625 nm (6 J), respectively. The higher the LSP pulse energy is, the more significant the left shift of the α peaks is.

3) The microhardness in the impact center increases with the LSP pulse energy and the value increases from HV 300 (before LSP) to HV 334 (2 J), to HV 342 (6 J). Meanwhile, after LSP with different laser pulse energy, the maximum residual stresses are -212 MPa (2 J) and -267 MPa (6 J), and the corresponding plastically affected depths are 680 μ m and 850 μ m, respectively.

References

[1] FOURIER J. Mechanical effects induced by shock waves generated by high-energy laser pulses [J]. *Mater Manuf Processes*, 1990, 5: 144–147.

- [2] YE C, SUSLOV S, KIM B J, STACH E A, CHENG G J. Fatigue performance improvement in AISI 4140 steel by dynamic strain aging and dynamic precipitation during warm laser shock peening [J]. *Acta Mater*, 2011, 59: 1014–1025.
- [3] ZHANG Y K, YOU J, LU J Z, CUI C Y, JIANG Y F, REN X D. Effects of laser shock processing on stress corrosion cracking susceptibility of AZ31B magnesium alloy [J]. *Surf Coat Technol*, 2010, 204: 3947–3953.
- [4] LIM H, KIM P, JEONG H, JEONG S. Enhancement of abrasion and corrosion resistance of duplex stainless steel by laser shock peening [J]. *J Mater Process Technol*, 2012, 212: 1347–1354.
- [5] SCHERPEREEL X, PEYRE P, FABBRO R, LEDERER G, CELATIL N. Modifications of mechanical and electrochemical properties of stainless steels surfaces by laser shock processing [J]. *Int Soc for Opt Eng*, 1997, 3097: 546–557.
- [6] CHU J P, RIGSBEE J M, BANAS G, ELSAYED-ALI H E. Laser-shock processing effects on surface microstructure and mechanical properties of low carbon steel [J]. *Mater Sci Eng A*, 1999, 260: 260–268.
- [7] ZHANG D, HARRIS S J, MCCARTNEY D G, PASHBY I R, POWELL J, SHIPWAY P H, VOISEY K T. The effect of laser transformation notching on the controlled fracture of a high carbon (C70S6) steel [J]. *Mater Sci Eng A*, 2008, 489: 273–284.
- [8] LU J Z, LUO K Y, ZHANG Y K, SUN G F, GU Y Y, ZHOU J Z, REN X D, ZHANG X C, ZHANG L F, CHEN K M, CUI C Y, JIANG Y F, FENG A X, ZHANG L. Grain refinement mechanism of multiple laser shock processing impacts on ANSI 304 stainless steel [J]. *Acta Mater*, 2010, 58: 5354–5362.
- [9] RUBIO G C, FELIX M C, GOMEZ R G, OCANA J L, MORALES M, PORRO J A. Effect of laser shock processing on fatigue crack growth of duplex stainless steel [J]. *Mater Sci Eng A*, 2011, 528: 914–919.
- [10] XIONG Y, HE T T, GUO Z Q, HE H Y, REN F Z, VOLINSKY A A. Effects of laser shock processing on surface microstructure and mechanical properties of ultrafine-grained high carbon steel [J]. *Mater Sci Eng A*, 2013, 570: 82–86.
- [11] FASISKA E J, WAGENBLAST T H. Dilation of alpha iron by carbon [J]. *TMS-AIME*, 1967, 239: 1818–1820.
- [12] FU W T, XIONG Y, ZHAO J, LI Y, FURUHARA T, MAKI T. Microstructural evolution of pearlite in eutectoid Fe-C alloys during severe cold rolling [J]. *J Mater Sci Technol*, 2005, 21: 25–27.
- [13] MONTROSS C S, WEI T, YE L, CLARK G, MAI Y W. Laser shock processing and its effects on microstructure and properties of metal alloys: a review [J]. *Int J Fatigue*, 2002, 24: 1021–1036.
- [14] KULKA M, PERTEK A. Laser surface modification of carburized and borocarbided 15CrNi6 steel [J]. *Mater Charact*, 2007, 58: 461–470.
- [15] LIU H, NAKATA K, ZHANG J X, YAMAMOTO N, LIAO J. Microstructural evolution of fusion zone in laser beam welds of pure titanium [J]. *Mater Charact*, 2012, 65: 1–7.
- [16] LUO K Y, LU J Z, ZHANG Y K, ZHOU J Z, ZHANG L F, DAI F Z, ZHONG J W, CUI C Y. Effects of laser shock processing on mechanical properties and micro-structure of ANSI 304 austenitic stainless steel [J]. *Mater Sci Eng A*, 2011, 528: 4783–4788.
- [17] ALTENBERGER I, SCHOLTES B, MARTIN U, OETTEL H. Cyclic deformation and near surface microstructures of shot peened or deep rolled austenitic stainless steel AISI 304 [J]. *Mater Sci Eng A*, 1999, 264: 1–16.
- [18] LINDEMANN J, BUQUE C, APPEL F. Effect of shot peening on fatigue performance of a lamellar titanium aluminide alloy [J]. *Acta Mater*, 2006, 54: 1155–1164.
- [19] MAAWAD E, SANO Y, WAGNER L, BROKMEIER H G, GENZEL C. Investigation of laser shock peening effects on residual stress state and fatigue performance of titanium alloys [J]. *Mater Sci Eng A*, 2012, 536: 82–91.
- [20] LARUE J E, DANIEWICZ S R. Predicting the effect of residual stress on fatigue crack growth [J]. *Int J Fatigue*, 2007, 29: 508–515.

(Edited by DENG Lü-xiang)